The Tudor protein Veneno assembles the ping-pong amplification complex that produces viral piRNAs in *Aedes* mosquitoes

Joep Joosten[1], Pascal Miesen[1], Bas Pennings[1], Pascal W. Jansen[2], Martijn A. Huynen[3], Michiel Vermeulen[2], and Ronald P. Van Rij[1+]

[1]Department of Medical Microbiology, Radboud Institute for Molecular Life Sciences, Radboud University Medical Center, P.O. Box 9101, 6500 HB Nijmegen, The Netherlands

[2]Department of Molecular Biology, Faculty of Science, Radboud Institute for Molecular Life Sciences, Radboud University Nijmegen, P.O. Box 9101, 6500 HB Nijmegen, The Netherlands

[3]Centre for Molecular and Bioinformatics, Radboud Institute for Molecular Life Sciences, Radboud University Medical Center, P.O. Box 9101, 6500 HB Nijmegen, The Netherlands

[+] corresponding author: ronald.vanrij@radboudumc.nl

Key words: piRNA, PIWI protein, Tudor, arbovirus, *Aedes aegypti*, Sindbis virus

ABSTRACT

Biogenesis of PIWI interacting RNAs (piRNAs) in *Drosophila melanogaster* and other model organisms relies on a myriad of co-factors, many of which belong to the Tudor protein family. In the vector mosquito *Aedes aegypti*, a somatically active piRNA pathway generates piRNAs *de novo* from cytoplasmic RNA viruses during an acute infection. In the *Ae. aegypti*-derived Aag2 cell line, piRNA biogenesis from alphaviruses and bunyaviruses requires ping-pong amplification by the PIWI proteins Ago3 and Piwi5. Thus far, the protein complex that mediates somatic piRNA biogenesis from exogenous, parasitic RNA remains unknown. We hypothesized that TUDOR-domain containing (Tudor) proteins are involved in vpiRNA production and thus performed a knockdown screen targeting all *Ae. aegypti* Tudor genes. Depletion of several Tudor proteins resulted in reduced vpiRNA production, with silencing of AAEL012441 having the most prominent and robust effect. This Tudor protein, which we named Veneno (Ven), interacts directly with Ago3 and localizes in cytoplasmic foci reminiscent of piRNA processing granules of *Drosophila*. Analyses of the Ven interactome reveals a network of additional co-factors including orthologues of the *Drosophila* piRNA pathway components Vasa (AAEL004978) and Yb (AAEL001939). Yb in turn interacts directly with Piwi5 and we propose that this multi-protein complex provides a molecular scaffold to allow efficient ping-pong amplification of vpiRNAs.

INTRODUCTION

In animals, three distinct small RNA-mediated silencing pathways exist: the micro (mi)RNA, small interfering (si)RNA and PIWI-interacting (pi)RNA pathways[1]. In all three, a small RNA molecule provides sequence specificity to guide a member of the Argonaute protein family to its target RNA. Whereas miRNAs and siRNAs associate with proteins of the AGO clade of this family, piRNAs are loaded onto PIWI clade proteins exclusively, forming piRNA induced silencing complexes (piRISCs)[2].

The piRNA pathway is primarily known for its role in transgenerational protection of genome integrity by silencing transposable elements in the germline[3,4]. Despite ubiquitous expression of piRNAs across metazoans, our knowledge on the molecular mechanisms that govern the piRNA pathway is limited to only a small number of model organisms[5]. In the *Drosophila melanogaster* germline, single-stranded precursors are produced from genomic piRNA clusters that contain remnants of transposable elements[6]. These precursors leave the nucleus and are processed to give rise to a pool of primary piRNAs. The PIWI proteins Piwi and Aubergine (Aub) are preferentially loaded with piRNAs that bear a uridine at the first nucleotide position (1U) and are generally antisense towards transposon mRNAs[6-8]. Piwi migrates to the nucleus to enforce transcriptional silencing, while Aub targets and cleaves cognate transposon RNA in an electron-dense perinuclear structure termed *nuage*[3,9]. The 3´-fragments that remain after Aub-cleavage are subsequently loaded onto the PIWI protein Ago3 and processed further into mature secondary piRNAs, which are primarily of sense orientation[6,7]. In turn, the resulting Ago3-piRISCs can target and cleave precursor transcripts to produce new antisense Aub-associated piRNAs, thus completing the so-called ping-pong amplification cycle. As Aub preferentially binds 1U piRNAs and cleaves target RNAs between nucleotides 10 and 11, Ago3-associated secondary piRNAs mostly have adenosine residues at their tenth nucleotide position (10A). The resulting overlap of 5' ends and 1U/10A nucleotide biases are hallmarks of piRNA production by the ping-pong amplification loop and are referred to as the ping-pong signature[6,7].

Ping-pong amplification of piRNAs was previously thought to be restricted to germline tissues, but recently, ping-pong dependent piRNA production has been demonstrated in somatic tissues of several arthropods, among which hematophagous mosquitoes of the *Aedes* family[10,11]. These anthropophilic vector mosquitoes, primarily *Ae. aegypti* and *Ae. albopictus*, are crucial for the transmission of several arthropod-borne (arbo)viruses that cause debilitating diseases such as dengue, chikungunya and Zika[12]. Since arboviral infectivity is greatly affected by the ability of the virus to replicate in the vector, mosquito antiviral immunity is a key determinant for virus transmission. Intriguingly, while causing severe disease in vertebrate hosts, arboviruses are able to replicate to high levels in the mosquito without apparent fitness cost to the insect[13]. An efficient immune response based on small interfering (si)RNAs is thought to contribute to this tolerance phenotype, as genetic interference with viral siRNA production causes elevated virus replication accompanied by increased mosquito mortality[14-17].

In addition to siRNAs, arbovirus infection results in *de novo* production of virus-derived piRNAs (vpiRNAs) in aedine mosquitoes and cell lines, suggesting that two independent small RNA pathways contribute to antiviral immunity in these insects[11]. In *Ae. aegypti* cells, vpiRNAs from the model alphavirus Sindbis virus (SINV) are predominantly produced in a ping-pong amplification loop involving the PIWI proteins Ago3 and Piwi5[18]. These proteins associate directly with vpiRNAs, which bear the distinct 1U/10A nucleotide signature indicative of ping-pong amplification.

The further configuration of protein complexes responsible for vpiRNA biogenesis is currently unknown. Moreover, it is unclear whether vpiRNA production requires dedicated complexes that differ from those that mediate biogenesis of piRNAs from other substrates (e.g. transposons or host mRNAs).

Studies in *D. melanogaster* and other model organisms have shown that TUDOR domain-containing (Tudor) proteins serve important functions in piRNA biogenesis, including the prevention of non-specific degradation of piRNA substrates, facilitating PIWI protein interactions, and aiding in small RNA loading onto specific PIWI proteins[3,4,19,20]. TUDOR domains contain conserved motifs that are known to interact with symmetrically dimethylated arginines (sDMAs), a common post-translational modification on PIWI proteins[21-23]. Consequently, Tudor proteins may serve as adapter molecules that facilitate the assembly of multi-molecular complexes involved in vpiRNA biogenesis in *Ae. aegypti*.

To test this hypothesis, we performed a functional knockdown screen of all predicted *Ae. aegypti* Tudor proteins, in which knockdown of the hitherto uncharacterized Tudor protein AAEL012441 shows the most prominent vpiRNA depletion. Because of this dramatic effect on vpiRNA biogenesis and the fact that its direct *D. melanogaster* orthologue (CG9684) is largely uncharacterized, we decided to focus our attention on this protein, which we named Veneno (Ven). Ven-depletion dramatically reduces piRNA production from both viral RNA strands, while ping-pong dependent piRNA production from endogenous sources (Ty3-gypsy transposons and histone H4 mRNA) is only mildly affected. Ven resides in cytoplasmic foci, reminiscent of piRNA processing granules in *Drosophila* and interacts directly with Ago3 through canonical TUDOR-domain mediated sDMA recognition. In addition, Ven associates with orthologues of *Drosophila* piRNA pathway components Vasa (AAEL004978) and Yb (AAEL001939)[9,24-29], which in turn binds Piwi5. We propose that this complex provides a molecular scaffold to support efficient ping-pong amplification of vpiRNAs by the PIWI proteins Ago3 and Piwi5.

MATERIALS AND METHODS

Tudor gene identification and orthologue detection

To allow comprehensive identification of all *Ae. aegypti* Tudor genes, we combined HHpred homology detection with Jackhmmer iterative searches[30,31]. Subsequently, we used T-Coffee to generate multiple sequence alignments to determine orthologous relations between *Ae. aegypti* and *D. melanogaster* Tudor proteins[32]. In view of the length of the Tudor domain (~50 AA) and low levels of sequence conservation among the family members we decided to use Neighbor Joining to identify orthology relations, which were consistent with the domain organization of the proteins. See Supplementary Information for a detailed description of our approach.

Transfection and infection of Aag2-cells

In knockdown experiments, cells were transfected with dsRNA and re-transfected 48 hours later to ensure prolonged knockdown. Where indicated, cells were infected with a recombinant Sindbis virus expressing GFP from a duplicated subgenomic promoter (SINV-GFP; produced from pTE3’2J-GFP[33,34]) at a multiplicity of infection (MOI) of 1 and harvested 48 hours post infection. For immunofluorescence (IFA) and immunoprecipitation (IP) experiments, Aag2

cells were transfected with expression plasmids encoding tagged transgenes and, where indicated, infected with SINV-GFP at an MOI of 1 three hours after transfection. All samples were harvested 48 hours after transfection. For mass spectrometry (MS) experiments, expression plasmids were transfected into cells using polyethylenimine (PEI) and infected 24 hours later with SINV (produced from pTE3'2J[33]) at an MOI of 0.1. MS-samples were harvested 72 hours post infection. For a more detailed description of cell culture conditions, generation of expression vectors, and virus production, see Supplementary Information.

Small RNA northern blotting and RT-qPCR

For small RNA northern blotting, RNA was size separated on polyacrylamide gels and cross-linked to nylon membranes using 1-ethyl-3-(3-dimethylaminopropyl)carbodiimide hydrochloride[35]. Small RNAs were detected using ^{32}P-labelled DNA oligonucleotides. For quantitative RT-qPCR analyses, DNaseI-treated RNA was reverse transcribed and PCR amplified in the presence of SYBR green. See Supplementary Information for a detailed description of the experimental procedures, sequences of probes used for northern blotting and qPCR primers.

Preparation of small RNA libraries and bioinformatic analyses

Total RNA from Aag2 cells transfected with dsRNA targeting either Veneno or Firefly Luciferase was used to generate small RNA deep sequencing libraries. For each condition, three transfections and library preparations were performed in parallel using Illumina's Truseq technology, as described in[36]. See Supplementary Information for additional details on the analyses of deep sequencing libraries.

Fluorescence and microscopy

Fluorescent imaging was performed on paraformaldehyde-fixed Aag2-cells that were permeabilized and counterstained using Hoechst-solution. Confocal images were taken using the Olympus FV1000 microscope. Images used for the quantification of GFP-signal granularity were taken using the Zeiss Axio Imager Z1 with ApoTome technology. See Supplementary Information for more details on the experimental approach.

Immunoprecipitation and western blotting

GFP- and RFP-tagged transgenes were immunoprecipitated using GFP- and RFP-TRAP beads (Chromotek), respectively, according to manufacturer's instructions. V5-tagged transgenes were purified using V5-agarose beads (Sigma), after pre-clearing the lysate on Protein A/G PLUS agarose beads (Santa Cruz). For Ago3 and Piwi5 immunoprecipitation (IP) experiments, antibodies targeting endogenous proteins were added to lysates at 1:10 dilution and incubated for 4 hours at 4ºC, followed by overnight binding to Protein A/G PLUS agarose beads (Santa Cruz). Protein extracts were resolved on polyacrylamide gels, blotted to nitrocellulose membranes, and probed with the indicated antibodies. Details on generation of Ago3 and Piwi5 antibodies, experimental procedures, and antibody dilutions can be found in the Supplementary Information.

Mass spectrometry

For mass spectrometry analysis, precipitated proteins were washed extensively and subjected to on-bead trypsin digestion as described previously[37]. Subsequently, tryptic peptides were acidified and desalted using Stagetips[38] before elution onto a NanoLC-MS/MS. Mass spectra were recorded on a QExactive mass spectrometer (Thermo Scientific). For details on the experimental procedures and the analyses of mass spectra, see Supplementary Information.

RESULTS

Comprehensive identification of Tudor proteins in *Aedes aegypti*

Tudor proteins play fundamental roles in the biogenesis of piRNAs in both vertebrate and invertebrate species[19,20]. We therefore hypothesized that processing of viral RNA into piRNAs in *Ae. aegypti* also involves members of this protein family. To faithfully identify all *Ae. aegypti* Tudor genes and their corresponding fly orthologues, we used a homology-based prediction approach combining HHPred and Jackhmmer algorithms[30,31]. First, we used HHPred homology detection to predict *D. melanogaster* TUDOR domain sequences, which were subsequently used as input for Jackhmmer iterative searches to identify all *D. melanogaster* and *Ae. aegypti* TUDOR domains. Ultimately, a neighbor joining tree was generated based on an alignment generated with T-Coffee[32], which enabled the identification of orthologous relationships between *Ae. aegypti* and *D. melanogaster* Tudor proteins (Figure 1).

Our analysis reveals that the majority of *Ae. aegypti* Tudor proteins cluster with a single *D. melanogaster* orthologue that has an identical domain composition. Some however (AAEL008834, AAEL008101, AAEL009987) lack clear one-to-one orthology with *Drosophila* counterparts, suggesting that these genes emerged as a result of duplication events that occurred after divergence of the *Drosophilidae* and *Culicidae* families. Alternatively, these proteins may have been lost from the *Drosophila* lineage, or the proteins may have diversified to an extent that they are no longer recognized as orthologous in the multiple sequence alignment. Similarly, CG15042 and Krimper are paralogous proteins in *D. melanogaster* that lack clear *Ae. aegypti* orthologues. Lastly, the *Ae. aegypti* genome encodes only one orthologue for the *D. melanogaster* Yb protein subfamily (Yb, SoYb and BoYb), namely AAEL001939.

Aedes aegypti Tudor proteins are involved in vpiRNA biogenesis

We included all identified *Ae. aegypti* Tudor proteins along with AAEL004290 in a functional knockdown screen. AAEL004290 is the orthologue of Eggless, a histone methyltransferase involved in the piRNA pathway in *D. melanogaster* which is predicted to contain TUDOR domains[39,40], although it did not surface in our HHpred-based homology detection.

In a previous study, deep sequencing of small RNAs from Sindbis-virus (SINV) infected Aag2 cells revealed that the majority of vpiRNAs are derived from a ~200nt hotspot in the SINV-capsid gene (Figure S1A)[18]. We selected four highly abundant sense (+) strand derived vpiRNA sequences from this hotspot region for small RNA northern blotting. Knockdown of several Tudor proteins lead to reduced vpiRNA levels in Aag2 cells, with knockdown of AAEL012441 resulting in the most prominent phenotype (Figure 2). This reduction cannot be explained by changes in viral replication, as only minor differences were seen in viral RNA levels across knockdowns under these experimental conditions (Figure 2 and S1B-C). Moreover, changes in vpiRNA production did not correlate with expression levels of capsid RNA, which is the source of vpiRNAs that we probed for in this screen (R^2=0.2276; Fig S1E). Knockdown

was generally efficient, resulting in a 50 to 80% reduction of mRNA abundance for most genes (Figure 2 and S1D). Interestingly, histone H4 mRNA-derived (+) piRNA production, which was previously shown to depend on amplification by Ago3 and Piwi5[41], was not affected by AAEL012441 knockdown (Figure 2), suggesting that this protein acts in a complex that preferentially processes piRNAs from viral transcripts. As depletion of AAEL012441 resulted in the most prominent reduction of vpiRNA levels in repeated experiments (Figure S2), we proceeded with a more detailed characterization of this protein. Since the word virus comes from the Latin word for poison, we named the Tudor protein that is required for production of piRNAs from viral RNA after the Spanish word for poison: Veneno (Ven).

Depletion of Veneno predominantly affects production of viral piRNAs

Small RNA northern blotting is suitable for the detection of only a handful of highly abundant piRNAs. To enable more comprehensive analyses of small RNA populations upon Ven knockdown, we prepared small RNA deep sequencing libraries from Aag2 cells infected with SINV. Depletion of Ven cells resulted in a considerable reduction of vpiRNAs, whereas viral siRNA levels were unaffected (Figure 3A). As reported previously[18], SINV-derived piRNAs exhibit the 1U/10A nucleotide bias indicative of ping-pong amplification (Figure 3A). The distribution of piRNAs across the viral genome and their size profile is unchanged (Figure S3), indicating that Ven is not directly responsible for triggering vpiRNA production or size determination of vpiRNAs. Intriguingly, levels of piRNAs mapping to the sense (+) strand of transposable elements increase, while those derived from the antisense (-) strand are reduced (Figure S4A). As the vast majority of all transposon-derived piRNAs in our libraries originate from Ty3-gypsy elements (Figure S4B), the effects seen in this family may dominate the overall phenotype of transposon piRNAs. Indeed, upon stratification of transposon-derived piRNAs into subclasses, we found that increased (+) piRNA production combined with reduced (-) piRNA production is specific for Ty3-gypsy-derived piRNAs (Figure 3B), whereas piRNA production from other classes of transposons is either unchanged or reduced (Figure 3C, S4C). Intriguingly, Ty3-gypsy elements comprise the only class of transposable elements that is processed into piRNAs by the ping-pong amplification loop, as is apparent from the strong ping-pong signature (Figure 3B, S4C). Depletion of Ven results in reduced levels of sense and antisense BEL-Pao element-derived piRNAs (Figure 3C), which comprise the second-largest group of transposon-derived piRNAs (Figure S4B). In contrast to piRNAs derived from Ty3-gypsy elements, BEL-Pao piRNAs lack a 1U/10A nucleotide signature (Figure 3C). Instead, both sense and antisense BEL-Pao-derived piRNAs are enriched for 1U, suggestion their production does not depend on ping-pong amplification but are the result of a primary piRNA biogenesis pathway. A slight increase in siRNA production is seen for all transposon subfamilies (Figure 3B-C, S4C), which may reflect a slight increase of transposon transcript levels upon Ven-KD. In accordance with northern blot analyses (Fig 2), histone H4 mRNA-derived piRNA levels were unchanged upon Ven-KD (Figure 3D). Taken together, these findings suggest that Ven plays a role in ping-pong dependent piRNA biogenesis from viral RNA, but mostly affects primary processing of transposon-derived piRNAs.

Veneno localizes to cytoplasmic foci

To further characterize the molecular function of Ven during vpiRNA biogenesis, we expressed GFP-tagged Ven and several domain mutants in Aag2 cells (Figure 4A). In the process of cloning these constructs, we noticed that the VectorBase (VB) annotation of the Ven-gene is erroneous. We used Sanger sequencing of PCR products to revise the current gene annotation (Figure S5), which was corroborated by recently published Aag2 transcriptome data[42].

Expression of GFP-tagged Ven reveals accumulation of the protein in cytoplasmic foci reminiscent of piRNA processing granules such as the *nuage* or Yb bodies in *D. melanogaster* (Figure 4B)[9,27]. We tentatively term these foci Ven-bodies. In our revised annotation, Ven contains an RNA recognition motif (RRM) at its amino terminus. A mutant in which this motif has been removed (C91) retains its localization in Ven-bodies (Figure 4C), suggesting that putative RNA-binding is not required for granule formation. Additionally, Ven contains a Zn-finger of the MYND-type, a class of Zn-fingers predominantly involved in protein-protein interaction[43]. Removal of this MYND-domain (C234) abolishes granular accumulation of Ven (Figure 4E).

Intrinsically disordered sequences have recently been shown to mediate RNA binding and regulate RNA metabolism[44]. Ven contains such an asparagine (N)-rich region directly upstream of the MYND-domain. A mutant in which this N-rich stretch is removed (C199) retains its localization in Ven-bodies (Figure 4D), which grants further support to the importance of the MYND-domain specifically for this granular localization pattern. Similarly, a Q-rich sequence directly downstream of the MYND-type Zn-finger is not sufficient for Ven-accumulation, as removal of the MYND domain alone disrupts Ven-body formation. Removal of the C-terminal (N670) or both TUDOR domains (N400) does not affect subcellular localization (Figure 4G-H). To allow a more comprehensive analysis of Ven-body localization across mutants, we traced the cytoplasmic GFP-signal of ~50 cells per transgene and quantified the coefficient of variance of this signal as a measure for granularity (Fig 4I). This analysis confirms that Ven-body accumulation is abolished upon removal of the MYND-type Zn-finger (Fig 4J). Altogether, these findings suggest the MYND-type Zn-finger enables Ven localization into specific Ven-bodies where components of the mosquito piRNA biogenesis machinery may be recruited for efficient piRNA production.

Veneno provides a molecular scaffold for a ping-pong amplification complex

As Ven is important for efficient ping-pong amplification of vpiRNAs (Figure 2-3), we hypothesized that the protein may serve as a scaffold to facilitate the interaction between the ping-pong partners Ago3 and Piwi5. To investigate this hypothesis, we immunoprecipitated GFP-tagged Ven and probed using antibodies recognizing endogenous Ago3 and Piwi5 (Figure S6A for antibody characterization). We found that Ven interacts with Ago3, but not Piwi5, regardless of the presence of an ongoing SINV-infection (Figure 5A). Immunoprecipitation of GFP alone does not copurify Ago3, confirming that the interaction is mediated by Ven (Figure 5A). To further dissect the multi-molecular network in which Ven participates, we employed quantitative mass spectrometry of immunoprecipitated GFP-Ven complexes from both uninfected and SINV-infected Aag2 cells. These data confirm the association with Ago3 and reveal interesting additional Ven-interactors (Figure 5B-C and Supplementary Table 1). Specifically, the orthologue of the Yb-subfamily, AAEL001939 is enriched in Ven-complexes immunoprecipitated from both mock- and SINV-infected cells. We verified these interactions by co-purifying its constituents in reciprocal IPs followed by western blot (Figure 5D). These immunoprecipitation experiments reveal that AAEL004978, the *Ae. aegypti* orthologue of

Vasa, also associates with Ven. Vasa is a DEAD-box helicase that in *Drosophila* recruits PIWI proteins to accommodate ping-pong amplification. Interestingly, we also detected Piwi5 as a direct interaction partner of Yb. Together, these findings reveal the presence of a multi-molecular complex in which the ping-pong partners Ago3 and Piwi5 are brought together by the Tudor proteins Ven and Yb (Figure 6E).

Ven-Ago3 interaction depends on sDMA-recognition

Interaction between TUDOR and PIWI proteins generally depends on recognition of symmetrically dimethylated arginines (sDMAs) on PIWI proteins by an aromatic cage encoded in the TUDOR domain[23]. To further characterize the domain required for the interaction between Ven and Ago3, we immunoprecipitated truncated Ven transgenes and assessed copurification of Ago3. A truncated Ven-mutant lacking the RRM (C206-Figure 6A) still strongly associates with Ago3 (Figure 6C). Moreover, this mutant retains its association in a complex involving Yb, Vasa and Piwi5 as shown by mass spectrometry (Figure S6B, Supplementary Table 2) and reciprocal IPs (Figure S6C). The MYND-domain mutant (C234), in which the distinct localization pattern is distorted (Figure 4), still aptly binds Ago3, suggesting that granular localization is not required for Ago3-interaction (Figure 6C). The carboxyl terminus containing two TUDOR domains (C400) is sufficient for interaction with Ago3, whereas Ago3-binding is lost upon deletion of the second (206-669) or both (206-399) Tudor domains (Figure 6C). However, this loss of binding may result from reduced expression or stability of these mutants (Figure 6C). Hence, to further specify whether Ven-Ago3 interaction is TUDOR domain mediated, we generated Ven transgenes carrying point mutations in residues predicted to be involved in sDMA recognition (2Δ: C206-G463A/Y465A and 4Δ: C206-G463A/Y465A/D483A/N486A; Figure 6B). We found that the second TUDOR domain of Ven is atypical in that only one of the residues that are predicted to be part of the aromatic cage is conserved (Figure S6D). We therefore only analyzed binding of Ago3 to Ven that carries point mutations in the first TUDOR domain. Interaction with Ago3 was lost in these mutants, suggesting that the first TUDOR domain of Ven binds Ago3 in a canonical sDMA-dependent manner (Figure 6C). It is likely that the C-terminal TUDOR domain is not involved in Ago3 binding since critical residues are not conserved (Figure S6D). However, we cannot fully exclude that cooperative binding of both TUDOR domains by Ago3 is required for efficient association with Ven. The interaction with Ago3 is not required for localization of Ven in Ven-bodies, as introducing the indicated point mutations (G463A/Y465A) in the context of the full length protein does not affect its subcellular localization pattern (Figure 6D). Altogether, our findings support a model in which Veneno, through sDMA recognition, recruits Ago3 to a multi-molecular complex that promotes ping-pong amplification of piRNAs preferentially from exogenous RNAs (Figure 6E).

DISCUSSION

Mosquito antiviral immunity largely relies on the processing of viral dsRNA into virus-derived siRNAs that direct degradation of viral RNAs. The discovery of *de novo* production of vpiRNAs from arboviral RNA however, uncovered the intriguing possibility of an additional small RNA-based line of defense against arboviruses. Processing of viral dsRNA into vsiRNAs by the siRNA pathway has been thoroughly characterized in mosquitoes[45,46]. As of yet, it is unclear how viral RNA produced in the cytoplasm is entered into the piRNA pathway, especially as canonical

substrates for the piRNA pathway are genomically encoded single-stranded precursors[3,4]. To better understand how viral RNA is processed by the mosquito piRNA pathway, more insight in the underlying mechanisms of vpiRNA biogenesis is needed.

In *Ae. aegypti*, vpiRNAs are amplified by the ping-pong partners Ago3 and Piwi5, but auxiliary proteins involved in this process remain enigmatic. As a tightly regulated network of Tudor proteins promotes production of piRNAs in *Drosophila*[19,20], we performed a comprehensive knockdown screen to evaluate the role of *Ae. aegypti* Tudor proteins in vpiRNA biogenesis. Knockdown of several Tudor genes affects vpiRNA biogenesis, with knockdown of Veneno (Ven) resulting in the strongest depletion of vpiRNAs. Additional candidates that reproducibly show depletion in vpiRNA levels are AAEL001939, the only orthologue of the *Drosophila* Yb-subfamily, and AAEL008101, which does not contain a one-to-one orthologue in the fruit fly. The fact that knockdown of these genes affects vpiRNA levels is especially compelling as knockdown efficiency was relatively low. Whereas AAEL001939 involvement in vpiRNA biogenesis is likely explained by its central place in the multi-protein complex discovered in this study, the molecular function of AAEL008101 remains to be elucidated. Involvement of additional Tudor proteins may be masked by redundancy of paralogous proteins or suboptimal knockdown efficiency.

Thus far, the direct orthologue of Ven in *D. melanogaster* (CG9684) has not been studied extensively. In a systematic analysis of all *Drosophila* Tudor proteins, germline-specific knockdown of CG9684 did not affect steady-state levels of transposon transcripts or female fertility rate[26]. This study, however, did not evaluate the effect of CG9684 knockdown on small RNA populations.

Ven accumulates in cytoplasmic foci similar to piRNA processing bodies in the fly. In *Drosophila* somatic follicle cells, which surround the germ cells, primary piRNA biogenesis takes place in Yb bodies. One of the core factors present in these structures is their eponym Yb[26-28]. Yet, no piRNA amplification takes place in Yb bodies, since the ping-pong partners Aub and Ago3 are not expressed in follicle cells[47,48]. In contrast, in *Drosophila* germ cells piRNA amplification takes place in the *nuage* and one of the core proteins of this perinuclear structure is the helicase Vasa[9,24,25]. In *Drosophila* and silkworm, Vasa is directly implicated in secondary piRNA amplification by preventing non-specific degradation of piRNA precursors and facilitating their transfer to PIWI proteins[24]. Yb is not present in *nuage* but it has been suggested that its function may be taken over by its paralogous family members: brother and sister of Yb (BoYb and SoYb respectively)[26]. In *Ae. aegypti* only one paralog of Yb is encoded (AAEL001939), which associates directly with Ven and Piwi5. The presence of a multi-protein complex including orthologues of Vasa and Yb supports the idea that Ven-bodies resemble *nuage*-like piRNA processing bodies. In a previous study, we did not detect pronounced localization of transgenic Ago3 and Piwi5 in foci[18] and formation of cytoplasmic foci was not required for Ven-Ago3 interaction. Thus, it is likely that PIWI proteins are transient shuttled to Ven-bodies for piRNA-precursor handover and subsequent piRNA maturation.

Similar to Veneno, the *Drosophila* Tudor protein Krimper localizes in perinuclear granules, which are lost upon deletion of the amino terminus of the protein[49,50]. While Krimper directly interacts with both partners in the ping-pong loop in flies (Ago3 and Aub), Ven associates exclusively with Ago3. Intriguingly, Krimper-Ago3 interaction is retained when using an arginine-methylation-deficient mutant of Ago3, whereas an sDMA-recognition-deficient

mutant of Ven is unable to bind Ago3. Thus, sDMA recognition seems to be required for Ven-Ago3 interaction in mosquitoes, but dispensable for Krimper-Ago3 association in fruit flies.

Knockdown of Ven greatly affects ping-pong dependent production of piRNAs derived from exogenous viral RNA. Intriguingly, Ven-KD has no effect on ping-pong dependent piRNA production from mRNAs (histone H4 RNA-derived piRNAs) and exclusively reduces 1U-biased transposon-derived piRNA levels (sense and antisense). The apparent stability of histone H4 derived piRNAs is especially surprising as their production has previously been shown to depend on ping-pong amplification, involving the PIWI proteins Ago3 and Piwi5[41]. These data suggest that Ven is involved in specifying the substrate for piRNA production and may preferentially shuttle viral RNA into the ping-pong loop. It would be interesting to assess whether viral RNA from other arbovirus families are similarly affected by Ven knockdown, which would point towards a more general role of Ven in self-nonself discrimination.

Dependency on specific co-factors for the biogenesis of small RNAs from different RNA sources is not unprecedented. For example, the siRNA pathway co-factor Loqs-PD is required for processing of endogenous siRNA-precursors, but is dispensable for siRNA production from exogenous dsRNA or viral RNA[51,52]. Another study showed that the Tudor protein Qin/Kumo specifically prevents (+) strand transposon RNAs from becoming Piwi-bound piRNAs during the process of piRNA phasing[53]. Analogies can also be drawn to the vertebrate piRNA pathway, where Tdrd1, the closest mouse orthologue of Ven, ensures processing of the correct transcripts by the piRNA pathway[54]. Accordingly, the PIWI protein Mili contains a disproportionally large population of piRNAs derived from cellular mRNA and ribosomal RNA in *Tdrd1* knockout mice. In a similar fashion, Ven could promote processing specifically of viral RNA by the mosquito piRNA pathway. Yet, we expect the molecular mechanism underlying this Tudor protein-guided sorting to be different as Tdrd1 interacts with Mili, the PIWI protein that predominantly binds 1U biased primary piRNAs, whereas Ven associates with Ago3, which mainly binds 10A biased secondary piRNAs.

A sophisticated network of accessory proteins that guides diverse RNA substrates into distinct piRISC complexes may be of particular importance in *Ae. Aegypti* as this mosquito species encodes an expanded PIWI gene family consisting of eight members[55,56], of which *Ago3* and *Piwi 4-6* are expressed in somatic tissues[57]. Moreover, the repertoire of RNA molecules that are processed into piRNAs is extended to include mRNA and viral RNA[11]. Tudor proteins like Veneno may therefore aid in streamlining piRNA processing and potentially allow flexible adaptation of the piRNA pathway in response to internal and external stimuli such as arbovirus infection.

ACKNOWLEDGEMENTS

We thank members of the van Rij laboratory for fruitful discussions and the Microscopic Imaging Centre of Radboudumc for access to, and support for confocal microscopy. Sequencing was performed by the GenomEast platform, a member of the “France Génomique” consortium (ANR-10-INBS-0009). We would also like to thank Gorben Pijlman, (University of Wageningen) for kindly providing the pPUbB-GW vector, Frank van Kuppeveld (Utrecht University) for the rabbit-anti-GFP antibody and the Carnegie Institution of Washington for the Drosophila Gateway Vector collection. This work is financially supported by a PhD fellowship from Radboud University Medical Center to PM, and a European Research Council Consolidator Grant under the European Union’s Seventh Framework Programme (grant number ERC CoG 615680) to RPvR.

REFERENCES

1 Ghildiyal, M. & Zamore, P. D. Small silencing RNAs: an expanding universe. *Nat Rev Genet* **10**, 94-108, doi:10.1038/nrg2504 (2009).

2 Meister, G. Argonaute proteins: functional insights and emerging roles. *Nat Rev Genet* **14**, 447-459, doi:10.1038/nrg3462 (2013).

3 Czech, B. & Hannon, G. J. One Loop to Rule Them All: The Ping-Pong Cycle and piRNA-Guided Silencing. *Trends in biochemical sciences* **41**, 324-337, doi:10.1016/j.tibs.2015.12.008 (2016).

4 Hirakata, S. & Siomi, M. C. piRNA biogenesis in the germline: From transcription of piRNA genomic sources to piRNA maturation. *Biochim Biophys Acta* **1859**, 82-92, doi:10.1016/j.bbagrm.2015.09.002 (2016).

5 Lim, R. S. & Kai, T. A piece of the pi(e): The diverse roles of animal piRNAs and their PIWI partners. *Semin Cell Dev Biol* **47-48**, 17-31, doi:10.1016/j.semcdb.2015.10.025 (2015).

6 Brennecke, J. *et al.* Discrete small RNA-generating loci as master regulators of transposon activity in Drosophila. *Cell* **128**, 1089-1103, doi:10.1016/j.cell.2007.01.043 (2007).

7 Gunawardane, L. S. *et al.* A slicer-mediated mechanism for repeat-associated siRNA 5' end formation in Drosophila. *Science* **315**, 1587-1590, doi:10.1126/science.1140494 (2007).

8 Cora, E. *et al.* The MID-PIWI module of Piwi proteins specifies nucleotide- and strand-biases of piRNAs. *RNA* **20**, 773-781, doi:10.1261/rna.044701.114 (2014).

9 Lim, A. K. & Kai, T. Unique germ-line organelle, nuage, functions to repress selfish genetic elements in Drosophila melanogaster. *Proceedings of the National Academy of Sciences of the United States of America* **104**, 6714-6719, doi:10.1073/pnas.0701920104 (2007).

10 Lewis, S. H. *et al.* Pan-arthropod analysis reveals somatic piRNAs as an ancestral defence against transposable elements. *Nature ecology & evolution* **2**, 174-181, doi:10.1038/s41559-017-0403-4 (2018).

11 Miesen, P., Joosten, J. & van Rij, R. P. PIWIs Go Viral: Arbovirus-Derived piRNAs in Vector Mosquitoes. *PLoS Pathog* **12**, e1006017, doi:10.1371/journal.ppat.1006017 (2016).

12 Kraemer, M. U. *et al.* The global distribution of the arbovirus vectors Aedes aegypti and Ae. albopictus. *Elife* **4**, e08347, doi:10.7554/eLife.08347 (2015).

13 Lambrechts, L. & Scott, T. W. Mode of transmission and the evolution of arbovirus virulence in mosquito vectors. *Proc Biol Sci* **276**, 1369-1378, doi:10.1098/rspb.2008.1709 (2009).

14 Myles, K. M., Wiley, M. R., Morazzani, E. M. & Adelman, Z. N. Alphavirus-derived small RNAs modulate pathogenesis in disease vector mosquitoes. *Proceedings of the National Academy of Sciences of the United States of America* **105**, 19938-19943, doi:10.1073/pnas.0803408105 (2008).

15 Samuel, G. H., Wiley, M. R., Badawi, A., Adelman, Z. N. & Myles, K. M. Yellow fever virus capsid protein is a potent suppressor of RNA silencing that binds double-stranded RNA. *Proceedings of the National Academy of Sciences of the United States of America* **113**, 13863-13868, doi:10.1073/pnas.1600544113 (2016).

16 Sanchez-Vargas, I. *et al.* Dengue virus type 2 infections of Aedes aegypti are modulated by the mosquito's RNA interference pathway. *PLoS Pathog* **5**, e1000299, doi:10.1371/journal.ppat.1000299 (2009).

17 Cirimotich, C. M., Scott, J. C., Phillips, A. T., Geiss, B. J. & Olson, K. E. Suppression of RNA interference increases alphavirus replication and virus-associated mortality in Aedes aegypti mosquitoes. *BMC Microbiol* **9**, 49, doi:10.1186/1471-2180-9-49 (2009).

18 Miesen, P., Girardi, E. & van Rij, R. P. Distinct sets of PIWI proteins produce arbovirus and transposon-derived piRNAs in Aedes aegypti mosquito cells. *Nucleic acids research* **43**, 6545-6556, doi:10.1093/nar/gkv590 (2015).
19 Siomi, M. C., Mannen, T. & Siomi, H. How does the royal family of Tudor rule the PIWI-interacting RNA pathway? *Genes Dev* **24**, 636-646, doi:10.1101/gad.1899210 (2010).
20 Pek, J. W., Anand, A. & Kai, T. Tudor domain proteins in development. *Development* **139**, 2255-2266, doi:10.1242/dev.073304 (2012).
21 Maurer-Stroh, S. *et al.* The Tudor domain 'Royal Family': Tudor, plant Agenet, Chromo, PWWP and MBT domains. *Trends in biochemical sciences* **28**, 69-74, doi:10.1016/S0968-0004(03)00004-5 (2003).
22 Kirino, Y. *et al.* Arginine methylation of Piwi proteins catalysed by dPRMT5 is required for Ago3 and Aub stability. *Nat Cell Biol* **11**, 652-658, doi:10.1038/ncb1872 (2009).
23 Liu, H. *et al.* Structural basis for methylarginine-dependent recognition of Aubergine by Tudor. *Genes Dev* **24**, 1876-1881, doi:10.1101/gad.1956010 (2010).
24 Xiol, J. *et al.* RNA clamping by Vasa assembles a piRNA amplifier complex on transposon transcripts. *Cell* **157**, 1698-1711, doi:10.1016/j.cell.2014.05.018 (2014).
25 Patil, V. S. & Kai, T. Repression of retroelements in Drosophila germline via piRNA pathway by the Tudor domain protein Tejas. *Curr Biol* **20**, 724-730, doi:10.1016/j.cub.2010.02.046 (2010).
26 Handler, D. *et al.* A systematic analysis of Drosophila TUDOR domain-containing proteins identifies Vreteno and the Tdrd12 family as essential primary piRNA pathway factors. *EMBO J* **30**, 3977-3993, doi:10.1038/emboj.2011.308 (2011).
27 Saito, K. *et al.* Roles for the Yb body components Armitage and Yb in primary piRNA biogenesis in Drosophila. *Genes Dev* **24**, 2493-2498, doi:10.1101/gad.1989510 (2010).
28 Olivieri, D., Sykora, M. M., Sachidanandam, R., Mechtler, K. & Brennecke, J. An in vivo RNAi assay identifies major genetic and cellular requirements for primary piRNA biogenesis in Drosophila. *EMBO J* **29**, 3301-3317, doi:10.1038/emboj.2010.212 (2010).
29 Zamparini, A. L. *et al.* Vreteno, a gonad-specific protein, is essential for germline development and primary piRNA biogenesis in Drosophila. *Development* **138**, 4039-4050, doi:10.1242/dev.069187 (2011).
30 Soding, J., Biegert, A. & Lupas, A. N. The HHpred interactive server for protein homology detection and structure prediction. *Nucleic acids research* **33**, W244-248, doi:10.1093/nar/gki408 (2005).
31 Finn, R. D. *et al.* HMMER web server: 2015 update. *Nucleic acids research* **43**, W30-38, doi:10.1093/nar/gkv397 (2015).
32 Di Tommaso, P. *et al.* T-Coffee: a web server for the multiple sequence alignment of protein and RNA sequences using structural information and homology extension. *Nucleic acids research* **39**, W13-17, doi:10.1093/nar/gkr245 (2011).
33 Hahn, C. S., Hahn, Y. S., Braciale, T. J. & Rice, C. M. Infectious Sindbis virus transient expression vectors for studying antigen processing and presentation. *Proceedings of the National Academy of Sciences of the United States of America* **89**, 2679-2683 (1992).
34 Saleh, M. C. *et al.* Antiviral immunity in Drosophila requires systemic RNA interference spread. *Nature* **458**, 346-350, doi:10.1038/nature07712 (2009).
35 Pall, G. S. & Hamilton, A. J. Improved northern blot method for enhanced detection of small RNA. *Nat Protoc* **3**, 1077-1084, doi:10.1038/nprot.2008.67 (2008).
36 van Cleef, K. W. *et al.* Mosquito and Drosophila entomobirnaviruses suppress dsRNA- and siRNA-induced RNAi. *Nucleic acids research* **42**, 8732-8744, doi:10.1093/nar/gku528 (2014).
37 Smits, A. H., Jansen, P. W., Poser, I., Hyman, A. A. & Vermeulen, M. Stoichiometry of chromatin-associated protein complexes revealed by label-free quantitative mass spectrometry-based proteomics. *Nucleic acids research* **41**, e28, doi:10.1093/nar/gks941 (2013).

38 Rappsilber, J., Mann, M. & Ishihama, Y. Protocol for micro-purification, enrichment, pre-fractionation and storage of peptides for proteomics using StageTips. *Nat Protoc* **2**, 1896-1906, doi:10.1038/nprot.2007.261 (2007).
39 Ishizu, H., Siomi, H. & Siomi, M. C. Biology of PIWI-interacting RNAs: new insights into biogenesis and function inside and outside of germlines. *Genes Dev* **26**, 2361-2373, doi:10.1101/gad.203786.112 (2012).
40 Clough, E., Moon, W., Wang, S., Smith, K. & Hazelrigg, T. Histone methylation is required for oogenesis in Drosophila. *Development* **134**, 157-165, doi:10.1242/dev.02698 (2007).
41 Girardi, E. *et al.* Histone-derived piRNA biogenesis depends on the ping-pong partners Piwi5 and Ago3 in Aedes aegypti. *Nucleic acids research*, doi:10.1093/nar/gkw1368 (2017).
42 Maringer, K. *et al.* Proteomics informed by transcriptomics for characterising active transposable elements and genome annotation in Aedes aegypti. *BMC genomics* **18**, 101, doi:10.1186/s12864-016-3432-5 (2017).
43 Gamsjaeger, R., Liew, C. K., Loughlin, F. E., Crossley, M. & Mackay, J. P. Sticky fingers: zinc-fingers as protein-recognition motifs. *Trends in biochemical sciences* **32**, 63-70, doi:10.1016/j.tibs.2006.12.007 (2007).
44 Calabretta, S. & Richard, S. Emerging Roles of Disordered Sequences in RNA-Binding Proteins. *Trends in biochemical sciences* **40**, 662-672, doi:10.1016/j.tibs.2015.08.012 (2015).
45 Gammon, D. B. & Mello, C. C. RNA interference-mediated antiviral defense in insects. *Curr Opin Insect Sci* **8**, 111-120, doi:10.1016/j.cois.2015.01.006 (2015).
46 Blair, C. D. & Olson, K. E. The role of RNA interference (RNAi) in arbovirus-vector interactions. *Viruses* **7**, 820-843, doi:10.3390/v7020820 (2015).
47 Malone, C. D. *et al.* Specialized piRNA pathways act in germline and somatic tissues of the Drosophila ovary. *Cell* **137**, 522-535, doi:10.1016/j.cell.2009.03.040 (2009).
48 Li, C. *et al.* Collapse of germline piRNAs in the absence of Argonaute3 reveals somatic piRNAs in flies. *Cell* **137**, 509-521, doi:10.1016/j.cell.2009.04.027 (2009).
49 Sato, K. *et al.* Krimper Enforces an Antisense Bias on piRNA Pools by Binding AGO3 in the Drosophila Germline. *Mol Cell* **59**, 553-563, doi:10.1016/j.molcel.2015.06.024 (2015).
50 Webster, A. *et al.* Aub and Ago3 Are Recruited to Nuage through Two Mechanisms to Form a Ping-Pong Complex Assembled by Krimper. *Mol Cell* **59**, 564-575, doi:10.1016/j.molcel.2015.07.017 (2015).
51 Marques, J. T. *et al.* Functional specialization of the small interfering RNA pathway in response to virus infection. *PLoS Pathog* **9**, e1003579, doi:10.1371/journal.ppat.1003579 (2013).
52 Hartig, J. V. & Forstemann, K. Loqs-PD and R2D2 define independent pathways for RISC generation in Drosophila. *Nucleic acids research* **39**, 3836-3851, doi:10.1093/nar/gkq1324 (2011).
53 Wang, W. *et al.* Slicing and Binding by Ago3 or Aub Trigger Piwi-Bound piRNA Production by Distinct Mechanisms. *Mol Cell* **59**, 819-830, doi:10.1016/j.molcel.2015.08.007 (2015).
54 Reuter, M. *et al.* Loss of the Mili-interacting Tudor domain-containing protein-1 activates transposons and alters the Mili-associated small RNA profile. *Nat Struct Mol Biol* **16**, 639-646, doi:10.1038/nsmb.1615 (2009).
55 Campbell, C. L., Black, W. C. t., Hess, A. M. & Foy, B. D. Comparative genomics of small RNA regulatory pathway components in vector mosquitoes. *BMC genomics* **9**, 425, doi:10.1186/1471-2164-9-425 (2008).
56 Lewis, S. H., Salmela, H. & Obbard, D. J. Duplication and Diversification of Dipteran Argonaute Genes, and the Evolutionary Divergence of Piwi and Aubergine. *Genome Biol Evol* **8**, 507-518, doi:10.1093/gbe/evw018 (2016).

57 Akbari, O. S. *et al.* The developmental transcriptome of the mosquito Aedes aegypti, an invasive species and major arbovirus vector. *G3 (Bethesda)* **3**, 1493-1509, doi:10.1534/g3.113.006742 (2013).

Figure 1. Orthologous Tudor proteins in *D. melanogaster* and *Ae. Aegypti* have largely conserved domain structures. On the left, the neighbor-joining tree generated from the multiple sequence alignment of the TUDOR domains from *Ae. aegypti* (red) and *D. melanogaster* (blue) Tudor proteins is shown. On the right, predicted domain structures of Tudor proteins are drawn schematically. Numbers at the top indicate protein length in amino acids. B-box, B-box type zinc finger (Zf) domain; C2CH, C2CH-type Zf domain; C2H2, C2H2-type Zf domain; DEAD, DEAD box domain; HA2, Helicase-associated domain; Hel-C, helicase C domain; KH, K homology RNA-binding domain; LOTUS, OST-HTH/LOTUS domain; MBD, Methyl-CpG-binding domain; MYND, MYND (myeloid, Nervy, DEAF-1)-type Zf domain; PHD, PHD-type Zf domain; RING, RING-type Zf domain; RMI1_N, RecQ mediated genome instability domain; RRM, RNA recognition motif; SMN, survival motor neuron domain; SNase¸ Staphylococcal nuclease homologue domain; UBA, ubiquitin associated domain.

Figure 2. Loss of vpiRNA production upon knockdown of several Tudor proteins. Individual Tudor genes were knocked down in Aag2 cells by transfection of dsRNA after which small RNA production of (+) strand Sindbis virus (SINV)- and histone H4 mRNA (H4)-derived piRNAs was assessed using northern blot analyses. U6 snRNA was used as a loading control. The heat map depicts relative changes in NSP4 and Capsid viral RNA abundance and Tudor/Piwi5 knockdown efficiencies as determined by RT-qPCR. All expression values were normalized to SINV-infected dsLuc control samples. Grey boxes indicate samples in which no RT-qPCR was performed.

Figure 3. Veneno is required for efficient biogenesis of vpiRNAs. (**A-C**) The sum of normalized read counts of 25-30 nt piRNAs (left), 21 nt siRNAs (middle) mapping to the Sindbis virus (SINV) genome (**A**), Ty3-gypsy transposons (**B**) or BEL-Pao transposons (**C**) upon knockdown of Veneno (dsVen) and control knockdown (Firefly Luciferase, dsLuc). Panels on the right show the nucleotide bias at each position in the 25-30 nt small RNA reads mapping to sense strand (upper panel) and antisense strand (lower panel) in dsLuc control libraries. (**D**) The sum of normalized read counts of 25-30 nt piRNAs mapping to histone H4 mRNA (left) and the corresponding nucleotide bias (right) of these small RNA reads mapping to the sense strand (upper panel) and antisense strand (lower panel) in dsLuc control libraries. For bar charts, read counts of three libraries were normalized to their corresponding library sizes and analyzed separately for the sense (black) and antisense (grey) strands. Bars indicate mean +/- standard deviation. Two-tailed student's t-test was used to determine statistical significance (* $P < 0.05$; ** $P < 0.01$, *** $P < 0.001$). To generate sequence logos, all reads of three independent dsLuc control libraries were combined (n = number of reads).

Figure 4. Veneno accumulates in cytoplasmic Ven-bodies. (**A**) Schematic representation of Veneno transgenes used in immunofluorescence experiments. (Full: amino acid [aa] 1-785; C91: aa 91-785; C199: aa 199-785; C234: aa 234-785; C400: aa 400-785; N670: aa 1-670; N400: aa 1-399; red lines indicate sequences of low amino acid complexity). (**B-H**) Representative confocal images of cells expressing transgenes depicted in (**A**). Scale bar represents 10µm. (**I**) The cytoplasm of 46-56 individual cells expressing GFP-tagged transgenes was traced as depicted and the mean and standard deviation of signal intensity was measured to calculate the coefficient of variation as a measure of signal granularity. (**J**) Scatter dot plot shows the GFP-signal granularity for individual cells; the red line depicts the mean.

Figure 5. Characterization of a multi-protein complex involving ping-pong partners. (A) Protein lysates from SINV-infected (+) and uninfected (-) Aag2 cells transfected with expression plasmids encoding GFP or GFP-Ven before (Input) and after GFP-immunoprecipitation (IP) were analyzed for (co)purification of endogenous Ago3 and Piwi5 as well as the GFP-tagged transgene by western blot. The asterisk indicates a non-specific band. **(B-C)** Identification of Ven-interacting proteins in lysates from both in mock- (**B**) and Sindbis virus (SINV)-infected Aag2 cells (**C**) by label-free quantitative (LFQ) mass spectrometry. Permutation-based FDR-corrected t-test was used to determine proteins that are statistically enriched in the Ven-IP. The LFQ-intensity of GFP-Ven IP over a control IP using the same lysate and non-specific beads ($\log_2$-transformed) is plotted against the $-\log_{10} P$ value. Interactors with an enrichment of $\log_2$ fold change > 4.3; $-\log_{10} P$ value > 1.5 are indicated. Proteins in the top right corner represent the bait protein in green (Ven) and its interactors. Orthologues of known piRNA biogenesis factors in *D. melanogaster* are indicated in red and interacting proteins present in both mock- and SINV-infected pulldowns are shown in **bold** font. Where available, interacting proteins were named according to their closest orthologue in *D. melanogaster*. In case of uncharacterized orthologous *Drosophila* proteins, we assigned the Vectorbase GeneID to the protein. (**D**) Reciprocal IPs of GFP-Ven, RFP-Vasa, V5-3xflag-Yb, Ago3 and Piwi5. Samples were probed with antibodies against GFP, RFP, FLAG, Ago3, Piwi5 and α-tubulin as indicated.

Figure 6. Ven-Ago3 interaction is mediated by sDMA-recognition. (**A**) Schematic representation of Veneno transgenes used in Ago3 co-IP experiments. (C206: amino acid [aa] 206-785; C234: aa 234-785; C400: aa 400-785; 206-669: aa 206-669; 206-399: aa 206-399; 2Δ: C206-G463A/Y465A; Full-2Δ: G463A/Y465A; 4Δ: C206-G463A/Y465A/D483A/N486A; red lines indicate sequences of low amino acid complexity. **(B)** Sequence of part of the first Tudor domain with residues indicated that were mutated in the 2Δ and 4Δ transgenes. Residues indicated in red are predicted to be involved in sDMA recognition. **(C)** Lysates from Aag2 cells expressing GFP-tagged Ven transgenes were subjected to GFP-IP and subsequently analyzed for co-purification of Ago3 by western blot. α-Tubulin serves as loading control. Asterisks indicate non-specific bands. **(D)** Representative confocal image of Aag2 cells expressing GFP-tagged Ven-2Δ-mutant; scale bar represents 10µm. **(E)** Schematic model of the identified multi-protein complex responsible for ping-pong amplification of exogenous (viral) and endogenous (transposable element, TE)-derived piRNAs.

Figure 1.

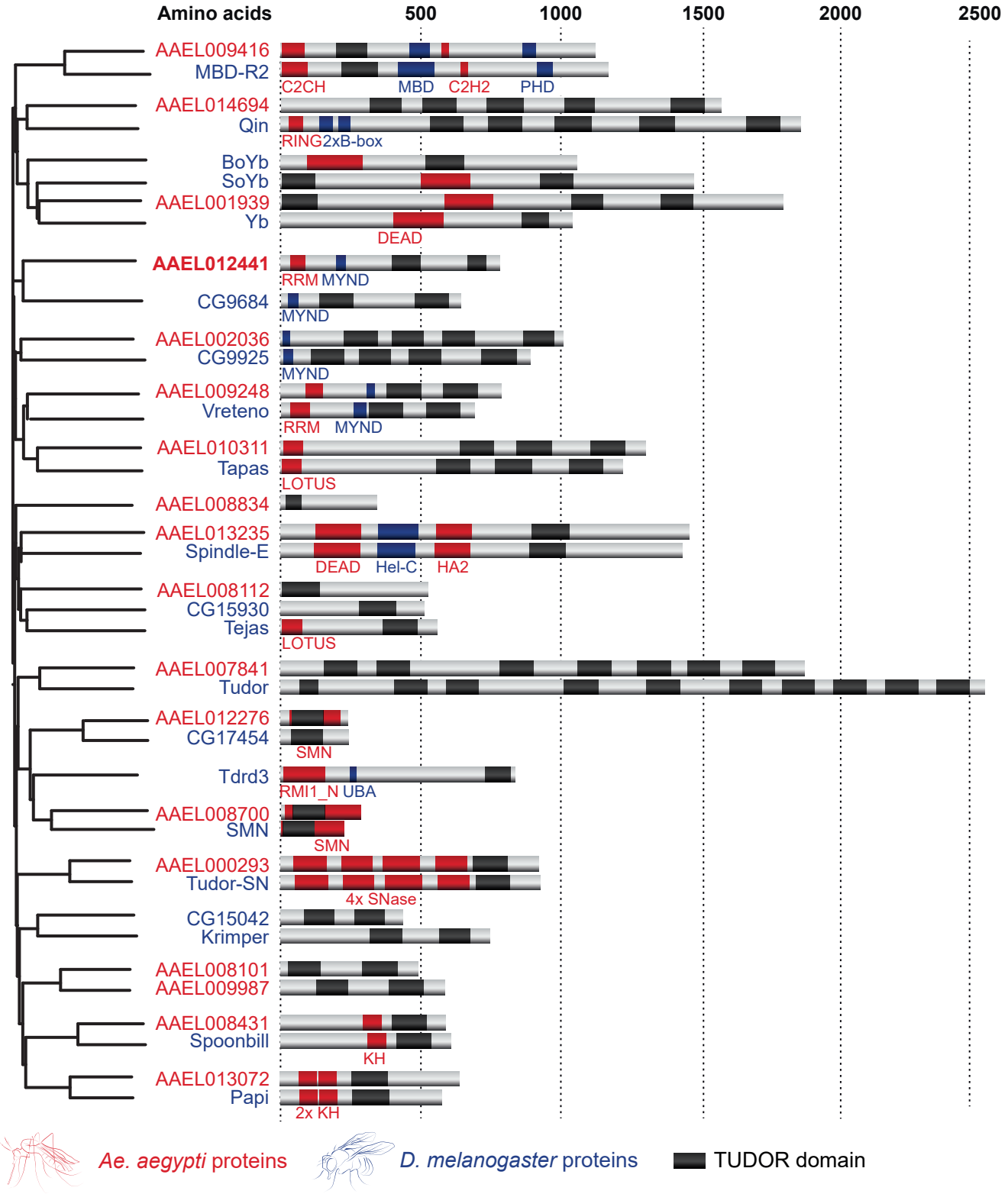
Amino acids
500
1000
1500
2000
2500
AAEL009416
MBD-R2
C2CH
MBD
C2H2
PHD
AAEL014694
Qin
RING
2xB-box
BoYb
SoYb
AAEL001939
Yb
DEAD
AAEL012441
RRM
MYND
CG9684
MYND
AAEL002036
CG9925
MYND
AAEL009248
Vreteno
RRM
MYND
AAEL010311
Tapas
LOTUS
AAEL008834
AAEL013235
Spindle-E
DEAD
Hel-C
HA2
AAEL008112
CG15930
Tejas
LOTUS
AAEL007841
Tudor
AAEL012276
CG17454
SMN
Tdrd3
RMI1_N
UBA
AAEL008700
SMN
SMN
AAEL000293
Tudor-SN
4x SNase
CG15042
Krimper
AAEL008101
AAEL009987
AAEL008431
Spoonbill
KH
AAEL013072
Papi
2x KH
Ae. aegypti proteins
D. melanogaster proteins
TUDOR domain

Figure 2

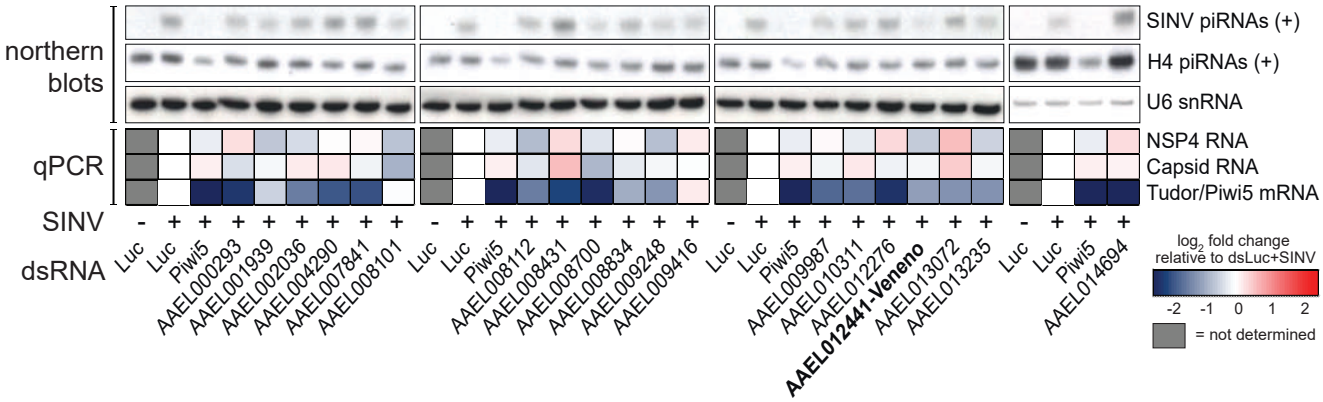
northern blots
qPCR
SINV piRNAs (+)
H4 piRNAs (+)
U6 snRNA
NSP4 RNA
Capsid RNA
Tudor/Piwi5 mRNA
SINV
dsRNA
Luc
Luc
Piwi5
AAEL000293
AAEL001939
AAEL002036
AAEL004290
AAEL007841
AAEL008101
Luc
Luc
Piwi5
AAEL008112
AAEL008431
AAEL008700
AAEL008834
AAEL009248
AAEL009416
Luc
Luc
Piwi5
AAEL009987
AAEL010311
AAEL012276
AAEL012441-Veneno
AAEL013072
AAEL013235
Luc
Luc
Piwi5
AAEL014694
log2 fold change relative to dsLuc+SINV
-2 -1 0 1 2
= not determined

Figure 3.

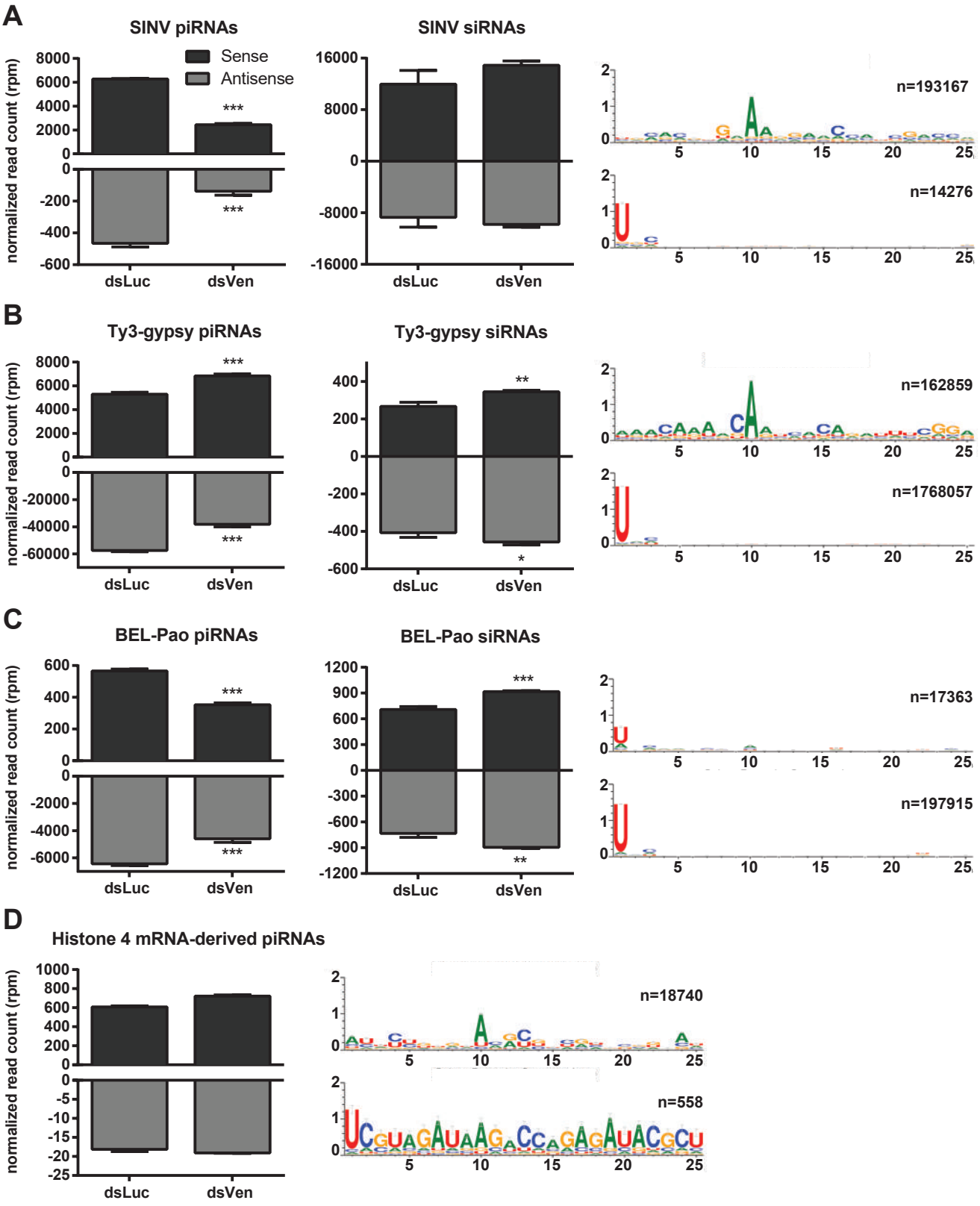
A
SINV piRNAs
SINV siRNAs
Sense
Antisense
normalized read count (rpm)
dsLuc
dsVen
n=193167
n=14276
B
Ty3-gypsy piRNAs
Ty3-gypsy siRNAs
n=162859
n=1768057
C
BEL-Pao piRNAs
BEL-Pao siRNAs
n=17363
n=197915
D
Histone 4 mRNA-derived piRNAs
n=18740
n=558

Figure 4.

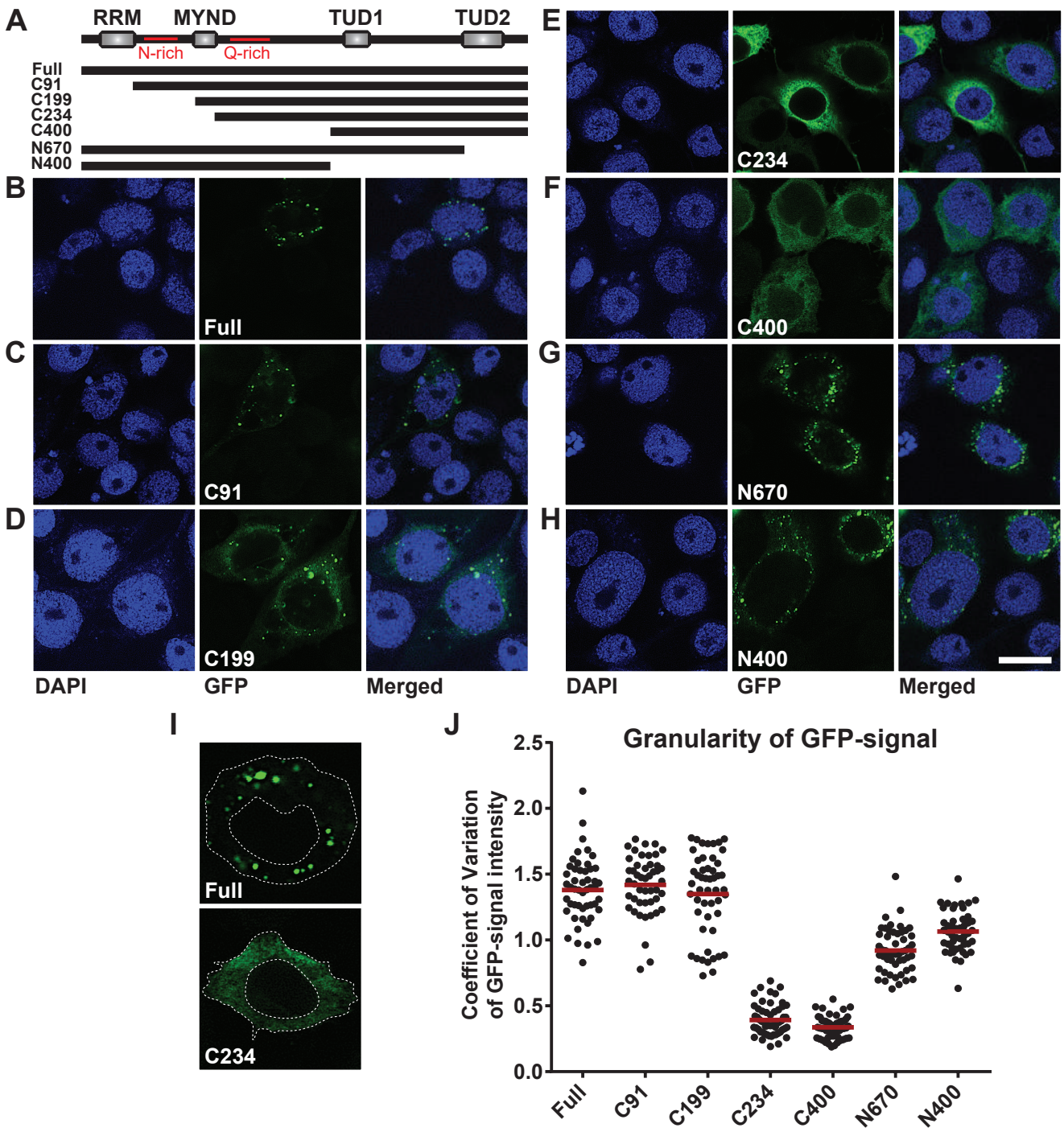
A
RRM
MYND
TUD1
TUD2
N-rich
Q-rich
Full
C91
C199
C234
C400
N670
N400
B
Full
C
C91
D
C199
DAPI
GFP
Merged
E
C234
F
C400
G
N670
H
N400
DAPI
GFP
Merged
I
Full
C234
J
Granularity of GFP-signal
Coefficient of Variation of GFP-signal intensity
2.5
2.0
1.5
1.0
0.5
0.0
Full
C91
C199
C234
C400
N670
N400

Figure 5.

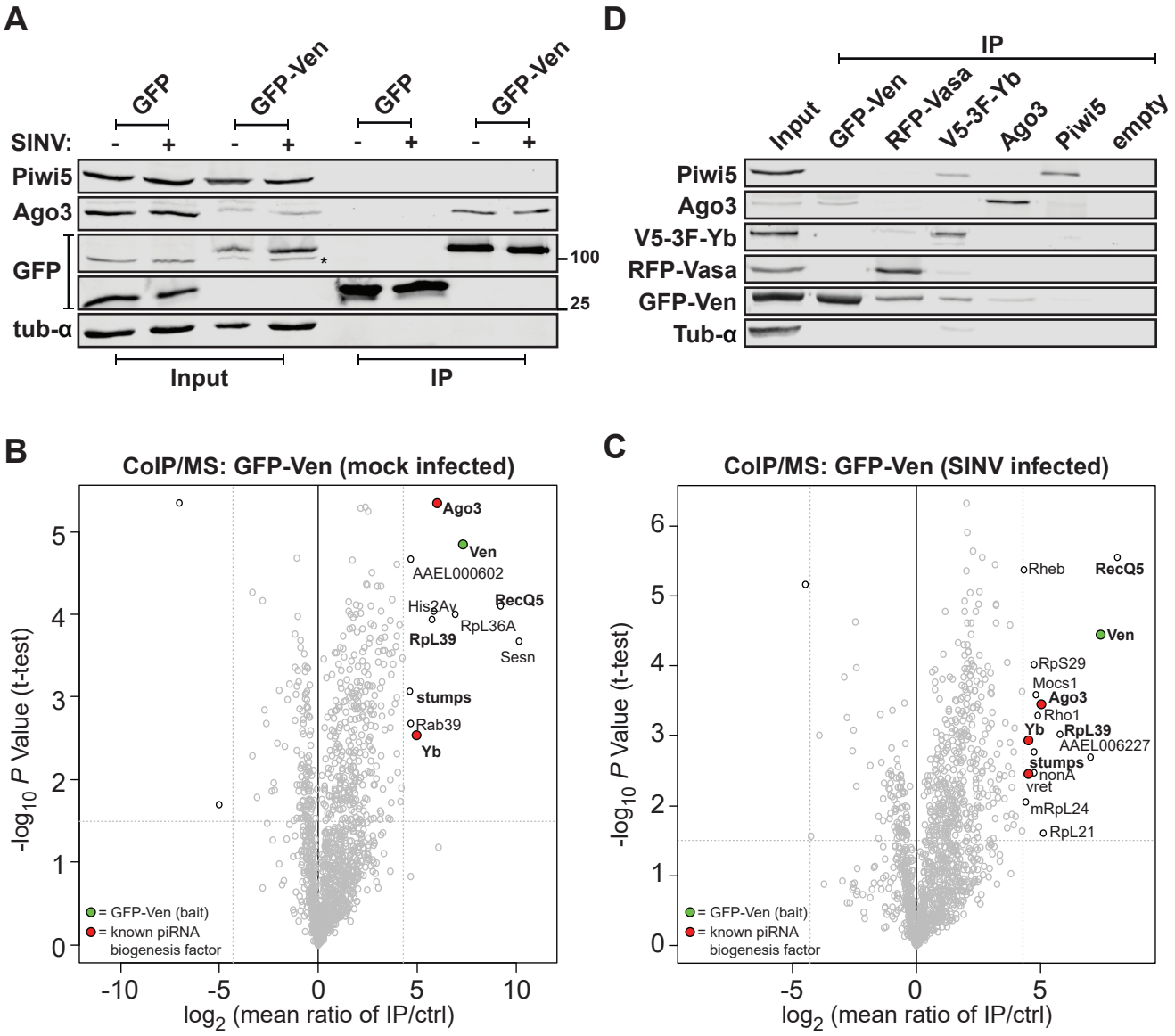
A
GFP
GFP-Ven
GFP
GFP-Ven
SINV:
- + - + - + - +
Piwi5
Ago3
GFP
tub-α
*
100
25
Input
IP
D
IP
Input
GFP-Ven
RFP-Vasa
V5-3F-Yb
Ago3
Piwi5
empty
Piwi5
Ago3
V5-3F-Yb
RFP-Vasa
GFP-Ven
Tub-α
B
CoIP/MS: GFP-Ven (mock infected)
Ago3
Ven
AAEL000602
RecQ5
His2Av
RpL36A
RpL39
Sesn
stumps
Rab39
Yb
= GFP-Ven (bait)
= known piRNA biogenesis factor
-log10 P Value (t-test)
log2 (mean ratio of IP/ctrl)
C
CoIP/MS: GFP-Ven (SINV infected)
Rheb
RecQ5
Ven
RpS29
Mocs1
Ago3
Rho1
Yb
RpL39
AAEL006227
stumps
nonA
vret
mRpL24
RpL21
= GFP-Ven (bait)
= known piRNA biogenesis factor
-log10 P Value (t-test)
log2 (mean ratio of IP/ctrl)

Figure 6.

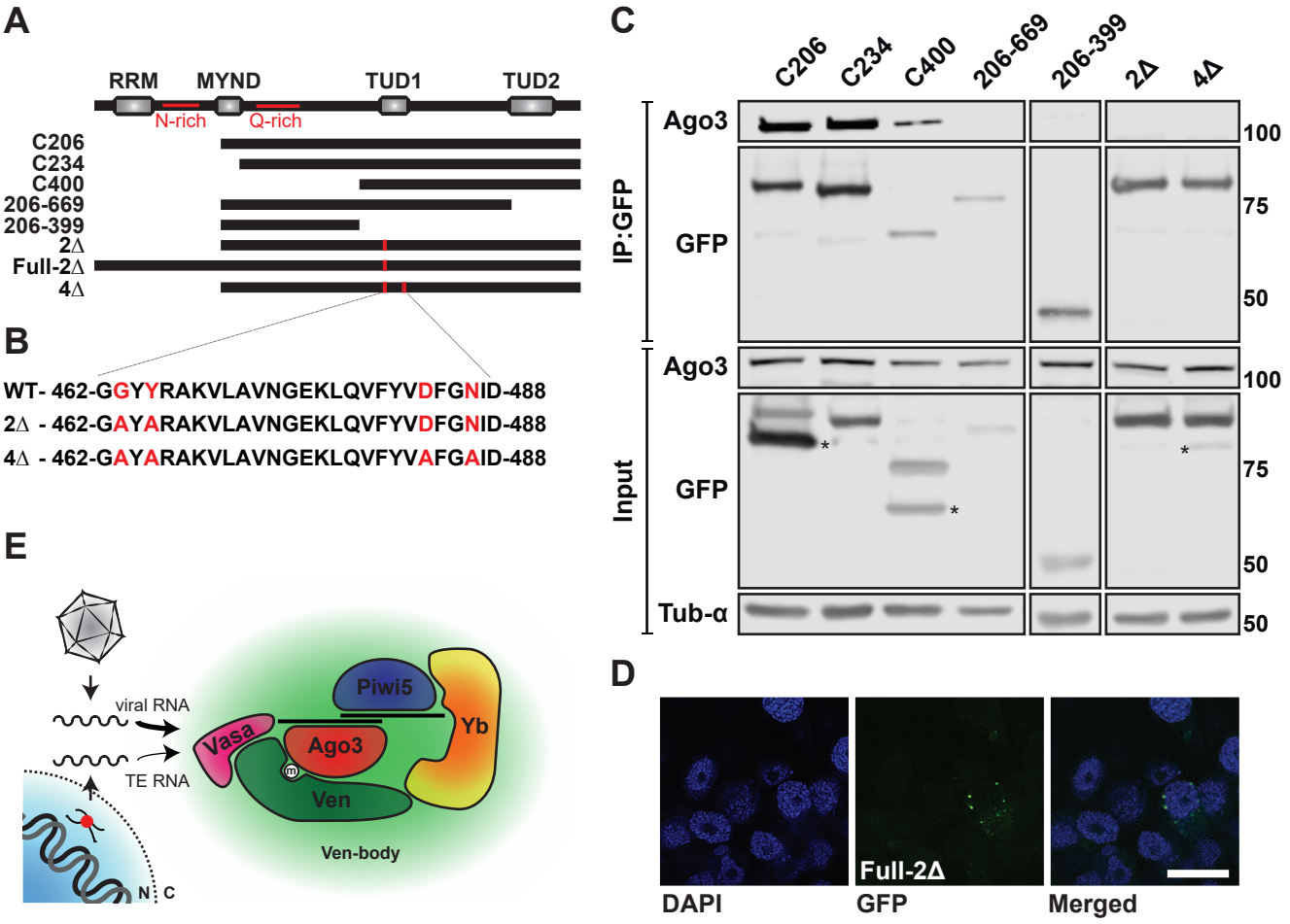
A
RRM
MYND
TUD1
TUD2
N-rich
Q-rich
C206
C234
C400
206-669
206-399
2Δ
Full-2Δ
4Δ
B
WT- 462-GGYYRAKVLAVNGEKLQVFYVDFGNID-488
2Δ - 462-GAYARAKVLAVNGEKLQVFYVDFGNID-488
4Δ - 462-GAYARAKVLAVNGEKLQVFYVAFGAID-488
C
C206
C234
C400
206-669
206-399
2Δ
4Δ
IP:GFP
Ago3
GFP
Input
Ago3
GFP
Tub-α
100
75
50
100
75
50
50
D
Full-2Δ
DAPI
GFP
Merged
E
viral RNA
TE RNA
Piwi5
Vasa
Ago3
Yb
Ven
Ven-body
N
C